
Supporting Information for

Topochemical Transformation Route to Atomically-thick Co_3O_4 Nanosheets Realizing Enhanced Lithium Storage Performance

Jinbao Zhu,[a] Liangfei Bai,[a] Yongfu Sun,[a] Xiaodong Zhang,[a] Qiuyang Li,[a] Boxiao Cao,[a] Wensheng Yan[b] and Yi Xie*[a]

[a] Division of Nanomaterials and Nanochemistry, Hefei National Laboratory for Physical Science at Microscale, University of Science and Technology of China, Hefei, Anhui, 230026, P.R. China.

* To whom correspondence should be addressed. Tel: +86 551-3603987 Fax: +86-551-3606266 E-mail: yxie@ustc.edu.cn.

[b] National Synchrotron Radiation Laboratory, University of Science and Technology of China, Hefei, Anhui 230029, P.R. China

Table of contents

S1. Experimental section

Synthesis of few-layered α-Co(OH)$_2$ nanosheets: All the reagents in the experiments were analytical grade and used in the preparation without further purification. In a typical experiment, cobalt chloride solution was added to ethylene glycol to reach a Co^{2+} concentration of 1.5 mM, after that concentrated ammonia was slowly dropped to the stirring pink solution (pH≈9.5) before being transferred to a Telflon-lined stainless steel autoclave and then heated in an electric oven at 130 °C for 24 h. After being cooled down to ambient temperature, the green cobalt hydroxide precursor was filtered and thoroughly washed with distilled water and ethanol several times. Then, the green obtained suspensions were added into a weighing bottle and then sonicated for 6 h. The resultant dispersions were harvested after centrifugation at 4000 rpm for 5 min. After centrifugation, the dispersions become almost transparent and the supernatant was further collected at high centrifuging velocity, and then obtained sample was dried at 60 °C in vacuum overnight.

Preparation of ATCNs: The ATCNs were prepared by topochemical transformation. In a typical procedure, 50 mg as-prepared few-layered α-Co(OH)$_2$ nanosheets was firstly added into ethanol to form a colloidal suspension, and then hydrogen peroxide solution (50 mL 3 wt%) was dropped into the suspension at 60 °C for 4 h. To remove possible nanoparticles after topochemical transformation, the resultant dispersions were firstly centrifuged at 2000 rpm for 20 minutes. After centrifugation, the supernatant was further collected by centrifuging the mixture at 12000 rpm for 5 minutes, and then dried in vacuum overnight for further characterization. Moreover, the bulk Co_3O_4 counterpart were also prepared by direct thermal decomposition cobalt nitrate hexahydrate at 800 °C for 24 h in air. For comparison with the ATCNs, the Co_3O_4 nanoparticles were also prepared by pyrolysis as-obtained few-layered α-Co(OH)$_2$ nanosheets at 600 °C for 5h in air.

Characterization

X-ray powder diffraction (XRD) patterns were recorded by using a Philips X’Pert Pro Super diffractometer with Cu Kα radiation (λ=1.54178 Å). The transmission electron microscopy (TEM) images were obtained by a Hitachi Model H-800 instrument with a tungsten filament. High-resolution transmission electron microscopy (HRTEM) images and electron diffraction (ED) patterns were carried out on a JEOL-2010 transmission electron microscope at an acceleration voltage of 200 kV. Atomic force microscopy (AFM) study in the present work was performed by means of Veeco DI Nano-scope MultiMode V system. Raman spectra were recorded at ambient temperature with a NEXUS 670 FT-IR Raman spectrometer. The nitrogen adsorption-desorption isotherms and corresponding pore size distribution were measured using a Micromeritics ASAP 2000 system at 77 K. AC electrochemical impedance measurements were performed using electrochemical station at room temperature (CHI660B). The synchrotron radiation X-ray absorption near edge structure (XANES) spectra was measured at the U19 beamline of the National Synchrotron Radiation Laboratory (NSRL).

Electrochemical measurements

The electrochemical measurements were carried out using home-made button cells with lithium metal as the counter and reference electrodes at room temperature. The electrode consisted of active material (ATCNs), conductivity agent (acetylene black), and polymer binder (polyvinylidene difluoride, PVDF) by a weight ratio of approximately 70:20:10. The dried material was coated on a copper foil and dried in a vacuum oven at 110 °C for 10 h, the active materials loading in each electrode was typically about 2 mg. The electrolyte was 1 M $LiPF_6$ in a 50:50 V/V mixture of ethylene carbonate/dimethyl carbonate (EC/DMC), and a microporous membrane (Celguard 2400, USA) as the separator. Cell assembly was carried out in an Ar-filled glove box and galvanostatic charge–discharge cycling performance was conducted at different current densities with a fixed voltage window between 3 V and 10 mV.

S2. The low magnification SEM image of ATCNs

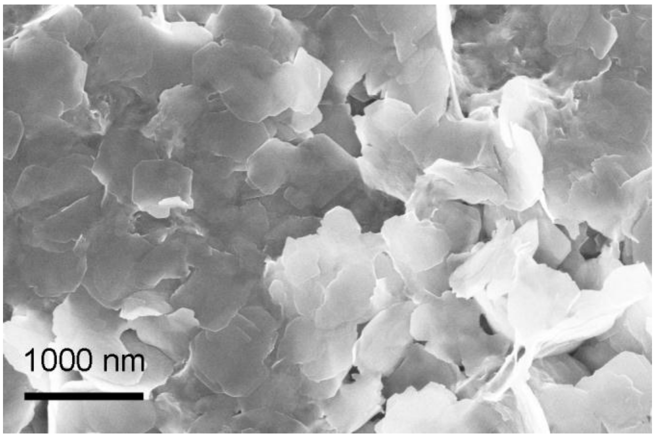

Figure S1. The typical panoramic SEM image of ATCNs and shows large-quantity of nanosheets with a size of about 400-600 nm

S3. Raman spectra of ATCNs compared with corresponding bulk counterpart

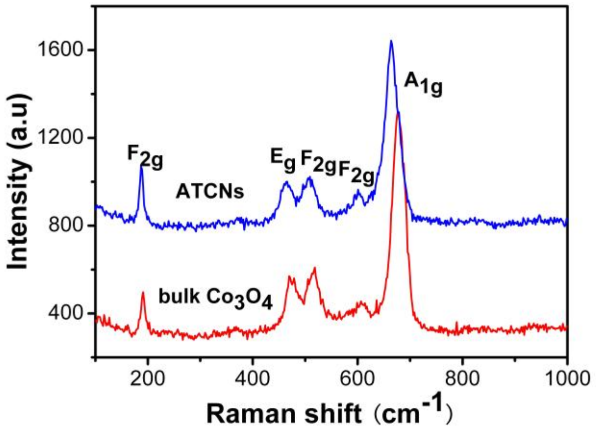

Figure S2. Raman spectra recorded from atomically-thick Co_3O_4 nanosheets (ATCNs) and bulk counterpart.

The five Raman active modes are observed in bulk Co_3O_4, which are consistent with the previous literature,[1] further confirming the high-quality cubic Co_3O_4. Obviously, the corresponding down-shifted Raman bands can be ascribed to the phonon confinement effect and the ultrathin thickness of the ATCNs.

S4. The N_2 adsorption-desorption isotherms and corresponding pore size distribution of ATCNs and Co_3O_4 nanoparticles

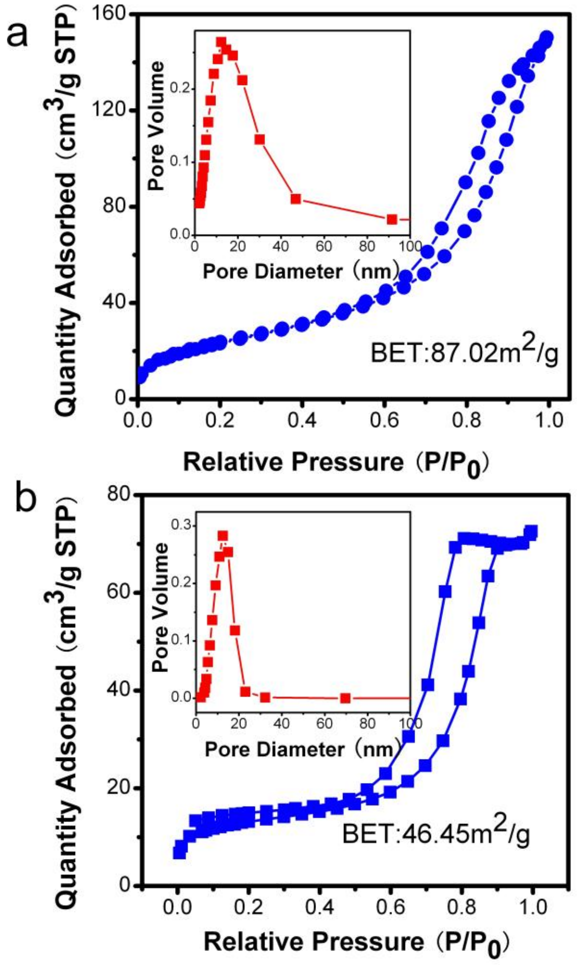

Figure S3. The N_2 adsorption-desorption isotherms and corresponding pore size distribution of a) ATCNs and b) Co_3O_4 nanoparticles calculated by Barretl-Joyner-Halenda (BJH) method from desorption branch.

The specific surface areas and porous nature of the products were further investigated by nitrogen adsorption/desorption measurements conducted at 77 K. The isotherms of ATCNs can be classified as type IV isotherms, revealing that the material is composed of aggregates (loose assemblages) of sheet-like particles forming slit-like pores.[2] The as-obtained ultrathin Co_3O_4 nanosheets have a huge Brunauer-Emmett-Teller (BET) surface area of 87.02 m^2/g with an average pore diameter of 12.2 nm and a pore volume of 0.235 cm^3/g (Figure S3a), higher than previously reported values of porous Co_3O_4 nanostructures and inorganic graphene analogues.[1, 3-7] However, the specific surface area of nanoparticles (Figure S3b) is only 46.45 m^2/g with an average pore diameter of 10 nm and a pore volume of 0.111 cm^3/g. The low surface areas of nanoparticles should be attributed to the larger crystal size resulting from aggregation in pyrolysis.

Owing to their unique morphology of finite in-plane size and well-defined layered structure, it is expected that laterally confined ultrathin nanosheets can significantly enhanced the host capabilities and cycling life of active electrode materials arising from highly enhanced surface areas and easier accessibilities of guest ions.[7, 8] In this case, the synergic advantages of atomically-thick Co_3O_4 nanosheets including both high specific surface areas and large inter-spacing volume, permitting adequate electrode-electrolyte contact and buffering the volume variation during cycling processes, are well-suited for electrochemical energy storage devices.

S5. The characteristic of few-layered α-$Co(OH)_2$ nanosheets

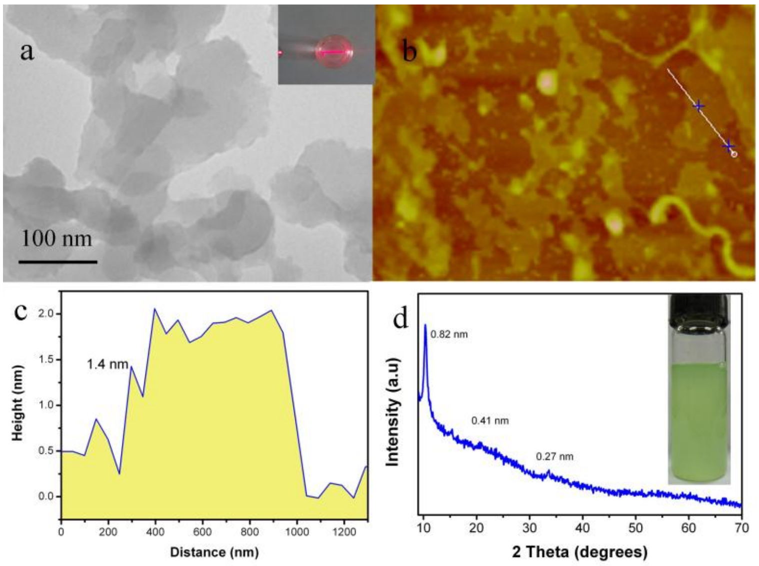

Figure S4. a) the TEM image of as-obtained few-layered α-$Co(OH)_2$ nanosheets, inset) photograph of a colloidal suspension of products. The suspension is side-illuminated to clearly demonstrate the typical Tyndall effect. b,c) The AFM image and the corresponding height profile of as-synthesized α-$Co(OH)_2$ nanosheets, providing solid evidence for the preparation of few-layered α-$Co(OH)_2$ nanosheets. d) The XRD pattern of few-layered α-$Co(OH)_2$ nanosheets-based film, the inset in panels d show bottle of the suspensions obtained by dispersing the sample in water.

The TEM image of as-obtained precursor clearly shows a large quantity of two-dimensional sheet-like structure, the darker areas can be attributed to overlapping of neighboring nanosheets and the nearly transparent feature indicates the ultrathin thickness (Figure S4a), which is further verified by the atomic force microscopic (AFM) image and corresponding height profile with a height of only 1.4 nm (Figure S4b,c). In general, the thickness observed by AFM is larger than that estimated from crystallographic data because of absorption of water and other systematic factors in the AFM measurements.[9] Thus, the present AFM result can be regarded as strong evidence for the preparation of few-layered $Co(OH)_2$ nanosheets. Meanwhile, the colloidal dispersions of the obtained products are highly stable over several weeks and display a typical Tyndall effect, reasonably indicating the formation of freestanding and homogeneous few-layer sheets (inset Figure S4a). Owing to the fact that it is currently infeasible to perform the X-ray diffraction pattern (XRD) characterization on a single nanosheet, a layer-by-layer assembly strategy was adopted to fabricate ultrathin nanosheets based film. The solely strong diffraction peak for the precursor can be readily assigned to the (003) facet of hydrotalcite-like phase (Figure S4d), while other small diffraction peaks can also be indexed to their (006) and (009) facets. This not only revealed the high orientation of the ultrathin nanosheets $Co(OH)_2$-based film, but also illustrated that the $Co(OH)_2$ ultrathin nanosheets had a preferred [001] orientation, Taken into the consideration its characteristic and color of green (inset Figure S4d), this precursor can be rationally identified as few-layered metastable α-$Co(OH)_2$ nanosheets.[10] It is well-known that layered cobalt hydroxides have two polymorphs: α- and β-$Co(OH)_2$. The α phase consists of stacked layers intercalated with various anions (such as CO_3^{2-},NO_3^-,Cl^-) and water molecules in the interlayer gallery, which thus has a larger interlayer spacing (>0.70 nm) than that of β-$Co(OH)_2$ (0.46 nm) without guest species.[11] Considerable efforts have been paid to preparation of single-layer/few-layer β-$Co(OH)_2$ nanosheets,[12] while the construction of few-layered metastable α-$Co(OH)_2$ remain great challenge and largely unexplored so far. Herein, we give the first case for the synthesis of novel (111)-oriented ATCNs with a thickness of only 1.5 nm via topochemical conversion from (001)-oriented few-layered α-$Co(OH)_2$ nanosheets, offering a new avenue to preparation of atomically-thick nanosheets for non-layered compounds.

S6. The XRD pattern and HRTEM image of Co_3O_4 nanoparticles

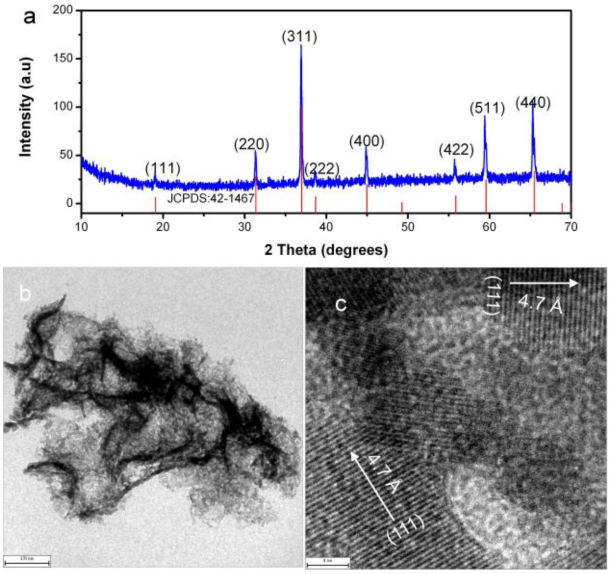

Figure S5. a) The XRD pattern of as-calcined Co_3O_4 nanoparticles, b) the TEM image and c) High-resolution TEM image of as-prepared Co_3O_4 nanoparticles.

All the XRD peaks could be perfectly assigned to the cubic spinel-type Co_3O_4 (a=8.08 Å JCPDS No.42-1467) without any undesirable phase within the experimental error (Figure

S5a). The thermal decomposition of precursors results in weight loss and volume shrinking and thus tends to deteriorate under high temperature calcinations, well crystallized and highly textured nanoparticles could be observed.[13] Figure S5b shows the TEM image of Co_3O_4 nanoparticles obtained by pyrolysis of few-layered α-cobalt hydroxide nanosheets in air. It clearly shows large quantity of Co_3O_4 nanoparticles with extremely small size about 5 nm. The obvious crystalline lattice with a distance of 4.7 Å matches very well with the lattice distance of (111) plane of cubic Co_3O_4, suggesting the similar growth behavior (Figure S5c).

S7. The cycling performance of ATCNs electrodes and Co_3O_4 nanoparticles at a rate of 1 C

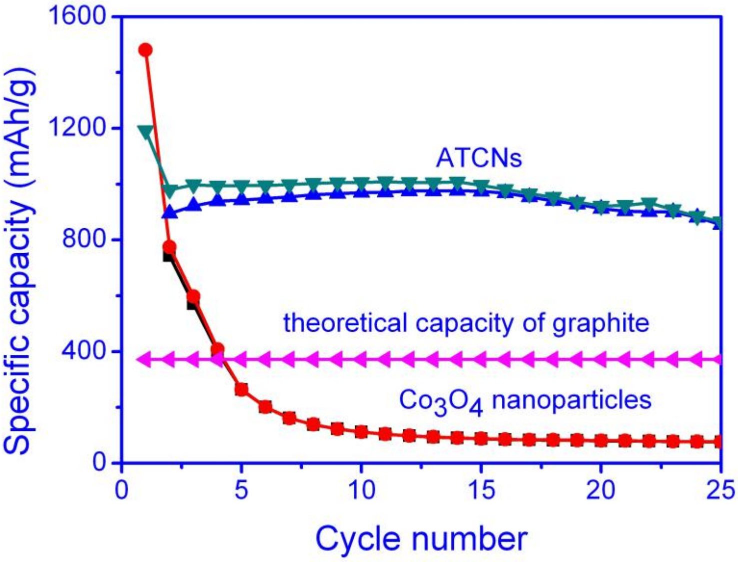

Figure S6. The cycling performance of ATCNs electrodes and Co_3O_4 nanoparticles at 1 C.

Considerable literatures have implied that IGAs electrodes cannot suffer from the high current density.[14] However, in this study, we find that the as-prepared ATCNs still exhibit the excellent lithium storage performance at fast charging, which is a remarkable advance for its practical application. A further increase in the C-rate to 1C leads to capacity loss per cycle (0.58%) and the discharge capacity reaches to 812.8 $mAh.g^{-1}$ after cycled, which is higher than of theoretical capacity of graphite and previously reported values for pure Co_3O_4 nanostructures, indicating the superiority of the ATCNs-based structure.[15-19] For comparison, the Co_3O_4 nanoparticles exhibit rapid capacity fading and remain only 76.5 mAh/g retention. Thus, the advantage of atomically-thick nanosheets for fast lithium storage is quite superior to nanoparticles at a large current density of 1C.

S8. Nyquist plots of ATCNs and nanoparticles after cycled

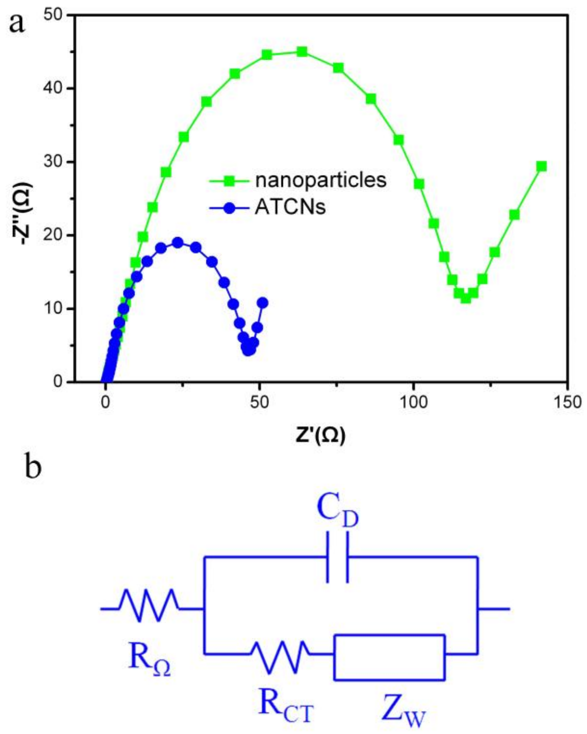

Figure S7. a) Nyquist plots of ATCNs and corresponding nanoparticles obtained by applying a sine wave with amplitude of 10.0 mV over the frequency range 100 kHz–0.1 Hz. b) Randles equivalent circuit for ATCNs and Co_3O_4 nanoparticles electrode/electrolyte interface. R_{Ω} is the ohmic resistance, CD is the double-layer capacitance, R_{CT} is the charge transfer resistance, and Z_W is the Warburg impedance describing the solid-state diffusion of Li^+ in Co_3O_4.[20]

In order to understand why ATCNs electrodes exhibit such a superior electrochemical performance compared to nanoparticles, AC impedance measurements were performed after cycled. The Nyquist plots show that the diameter of the semicircle for ATCNs in the high–medium frequency region is much smaller than that of Co_3O_4 nanoparticles, which suggests that ATCNs possess lower contact and charge-transfer resistances (Figure S7a).[21] It can be seen that the low-frequency tail for the three samples was also different, which can be compared qualitatively with reference to the mass (mainly of lithium ions) transfer kinetics in the electrodematerials. The low-frequency slope for the ATCNs composite electrode, higher than that of Co_3O_4 nanoparticles. The steeper low-frequency tail indicates higher lithium ion conductivity in the electrodematerials.[22] As expected, it indicates that the ATCNs composite electrode possesses a high electrical conductivity, a rapid charge-transfer process, and good Li-ion kinetics for lithium uptake and extraction. Therefore, the ATCNs composite exhibits outstanding lithium storage behavior compared to the Co_3O_4 nanoparticles.

References

1. S. L. Xiong, C. Z. Yuan, M. F. Zhang, B. J. Xi and Y. T. Qian, *Chem-Eur J*, 2009, **15**, 5320-5326.
2. C. Wang, Y. Zhou, M. Y. Ge, X. B. Xu, Z. L. Zhang and J. Z. Jiang, *J Am Chem Soc*, 2010, **132**, 46-+.
3. X. L. Xiao, X. F. Liu, H. Zhao, D. F. Chen, F. Z. Liu, J. H. Xiang, Z. B. Hu and Y. D. Li, *Adv Mater*, 2012, **24**, 5762-5766.
4. L. Tian, H. L. Zou, J. X. Fu, X. F. Yang, Y. Wang, H. L. Guo, X. H. Fu, C. L. Liang, M. M. Wu, P. K. Shen and Q. M. Gao, *Adv Funct Mater*, 2010, **20**, 617-623.
5. C. C. Li, X. M. Yin, Q. H. Li, L. B. Chen and T. H. Wang, *Chem-Eur J*, 2011, **17**, 1596-1604.
6. F. M. Zhan, B. Y. Geng and Y. J. Guo, *Chem-Eur J*, 2009, **15**, 6169-6174.
7. J. W. Seo, Y. W. Jun, S. W. Park, H. Nah, T. Moon, B. Park, J. G. Kim, Y. J. Kim and J. Cheon, *Angew Chem Int Edit*, 2007, **46**, 8828-8831.
8. J. T. Jang, S. Jeong, J. W. Seo, M. C. Kim, E. Sim, Y. Oh, S. Nam, B. Park and J. Cheon, *J Am Chem Soc*, 2011, **133**, 7636-7639.
9. R. Z. Ma and T. Sasaki, *Adv Mater*, 2010, **22**, 5082-5104.
10. Z. P. Liu, R. Z. Ma, M. Osada, K. Takada and T. Sasaki, *J Am Chem Soc*, 2005, **127**, 13869-13874.
11. X. Liu, R. Ma, Y. Bando and T. Sasaki, *Angew Chem Int Ed Engl*, 2010, **49**, 8253-8256.
12. X. H. Liu, R. Z. Ma, Y. Bando and T. Sasaki, *Adv Mater*, 2012, **24**, 2148-2153.
13. X. W. Lou, D. Deng, J. Y. Lee, J. Feng and L. A. Archer, *Adv Mater*, 2008, **20**, 258-+.
14. D. Rangappa, K. D. Murukanahally, T. Tomai, A. Unemoto and I. Honma, *Nano Lett*, 2012, **12**, 1146-1151.
15. S. Q. Chen and Y. Wang, *J Mater Chem*, 2010, **20**, 9735-9739.
16. W. Y. Li, L. N. Xu and J. Chen, *Adv Funct Mater*, 2005, **15**, 851-857.
17. Y. Liu, C. H. Mi, L. H. Su and X. G. Zhang, *Electrochim Acta*, 2008, **53**, 2507-2513.
18. Z. Z. Lin, W. B. Yue, D. Z. Huang, J. Y. Hu, X. Y. Zhang, Z. Y. Yuan and X. J. Yang, *Rsc Adv*, 2012, **2**, 1794-1797.
19. Y. G. Li, B. Tan and Y. Y. Wu, *Nano Lett*, 2008, **8**, 265-270.
20. Y. M. Lin, P. R. Abel, A. Heller and C. B. Mullins, *J Phys Chem Lett*, 2011, **2**, 2885-2891.
21. S. B. Yang, X. L. Feng and K. Mullen, *Adv Mater*, 2011, **23**, 3575-+.
22. G. M. Zhou, D. W. Wang, L. C. Yin, N. Li, F. Li and H. M. Cheng, *Acs Nano*, 2012, **6**, 3214-3223.